

Supplementary Materials for

Electrotunable artificial molecules based on van der Waals heterostructures

Zhuo-Zhi Zhang, Xiang-Xiang Song, Gang Luo, Guang-Wei Deng, Vahid Mosallanejad, Takashi Taniguchi, Kenji Watanabe, Hai-Ou Li, Gang Cao, Guang-Can Guo, Franco Nori, Guo-Ping Guo

Published 20 October 2017, *Sci. Adv.* **3**, e1701699 (2017)
DOI: 10.1126/sciadv.1701699

This PDF file includes:

- Supplementary Text
- fig. S1. Source-drain current, I_{SD} , versus the global back-gate voltage, V_{BG} .
- fig. S2. Tunability of the gate DM over a wider range at $V_{BG} = 30$ V.
- fig. S3. Tunability of the gate DM in another similar sample.
- fig. S4. COMSOL simulation of the interdot barrier.
- fig. S5. COMSOL simulation on the potential well distribution for different values of V_{DM} .
- fig. S6. Gate controllability in the low-density regime.
- Reference (58)

Supplementary Text

1. Source-Drain current I_{SD} versus the global Back-Gate voltage V_{BG}

A DC voltage was applied to the global back gate to tune the Fermi energy of the MoS₂ device without any local bottom gates voltage applied. The source-drain current (I_{SD}) was measured when sweeping the back-gate voltage (V_{BG}) at a fixed source-drain voltage (V_{SD}) of 5 mV. As shown in fig. S1, the device shows a typical n-type semiconductor behavior. The demonstration of the double quantum dot is presented above the turn-on threshold voltage, with an estimated field-effect mobility of ~ 300 cm²/(V•s). The estimated charge density at $V_{BG} = 25$ V and 30 V is 2.77×10^{11} cm⁻² and 1.20×10^{12} cm⁻², respectively.

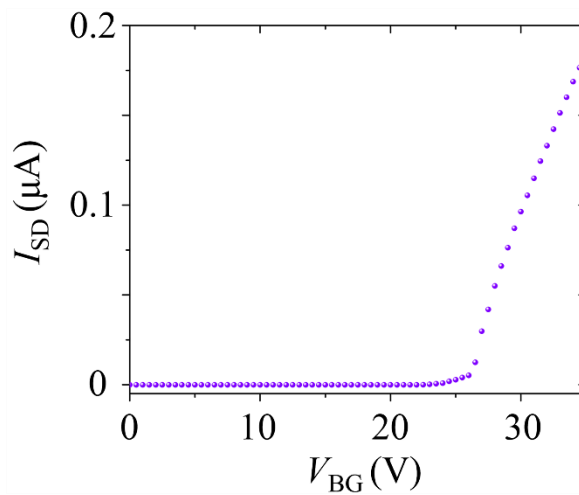


fig. S1. Source-drain current, I_{SD} , versus the global back-gate voltage, V_{BG} .

Without any local bottom gates voltage applied, the source-drain current I_{SD} was measured when sweeping the global back-gate voltage V_{BG} . The I_{SD} versus V_{BG} curve shows a typical n-type semiconductor behavior.

2. Tunability of the gate DM over a wider range

When tuning V_{DM} to a negative range, varying from -0.2 V to -1.2 V, while all other gate voltages remain fixed, one large quantum-dot atom evolves into a double-quantum-dot molecule. Figure S2 shows a typical area of the charge stability diagram, which is much larger than that shown in Fig. 3. Figure S3 shows a similar phenomenon observed in another sample.

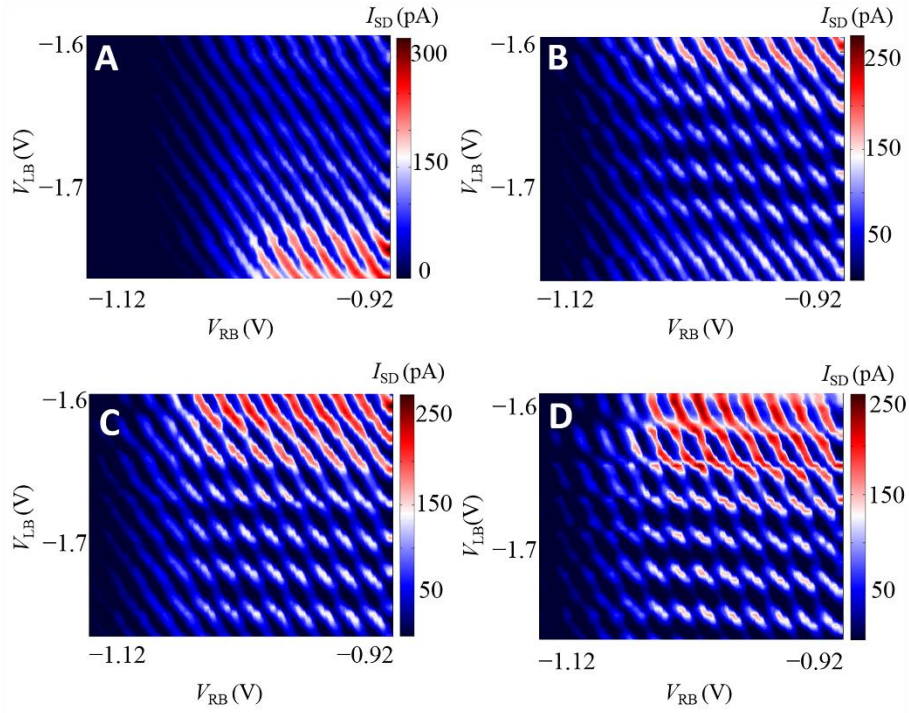


fig. S2. Tunability of the gate DM over a wider range at $V_{BG} = 30$ V. Current through the double quantum dot versus V_{LB} and V_{RB} applied to the gates LB and RB for $V_{BG} = 30$ V, $V_{LP} = V_{RP} = 0$ V, $V_{UM} = -2.1$ V, bias voltage at $V_{SD} = 100$ μ V and $V_{DM} = -0.2$ V, -1 V, -1.1 V and -1.2 V for **A** to **D**, respectively.

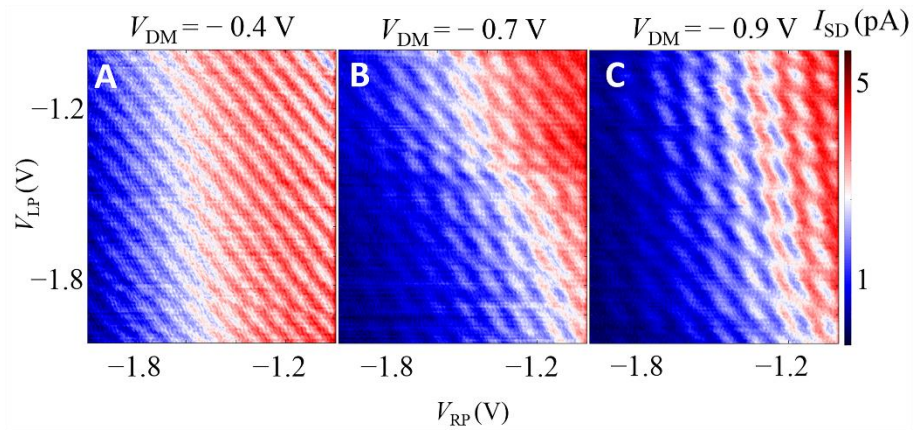


fig. S3. Tunability of the gate DM in another similar sample. Current through the double quantum dot versus V_{LP} and V_{RP} applied to the gates LP and RP, for $V_{BG} = 40$ V, $V_{LB} = V_{RB} = -0.64$ V, $V_{UM} = -1.1$ V, bias voltage at $V_{SD} = 100$ μ V and $V_{DM} = -0.4$ V, -0.7 V and -0.9 V for **A** to **C**, respectively. This data was measured from another sample with same structure.

3. Rough fitting of the fractional peak splitting f versus the gate voltage V_{DM}

Consider the inter-dot potential barrier in a parabolic form, $U(x) = -\frac{1}{2}kx^2$, the inter-dot coupling strength which corresponds to the transmission coefficient D can be determined (58) as $D = 1/(1 + e^{-2\pi\epsilon})$, where $\epsilon = (E/\hbar)\sqrt{m/k}$. We can roughly fit the fractional peak splitting f versus the gate voltage V_{DM} with a $1/(1 + e^{-kx})$ lineshape. It is worth noticing that in the strongly-coupled regime, the inter-dot potential barrier does not fit the quasi-classical model because of the high value of the transmission coefficient. So the fit is not suitable when the value of V_{DM} is near 0.

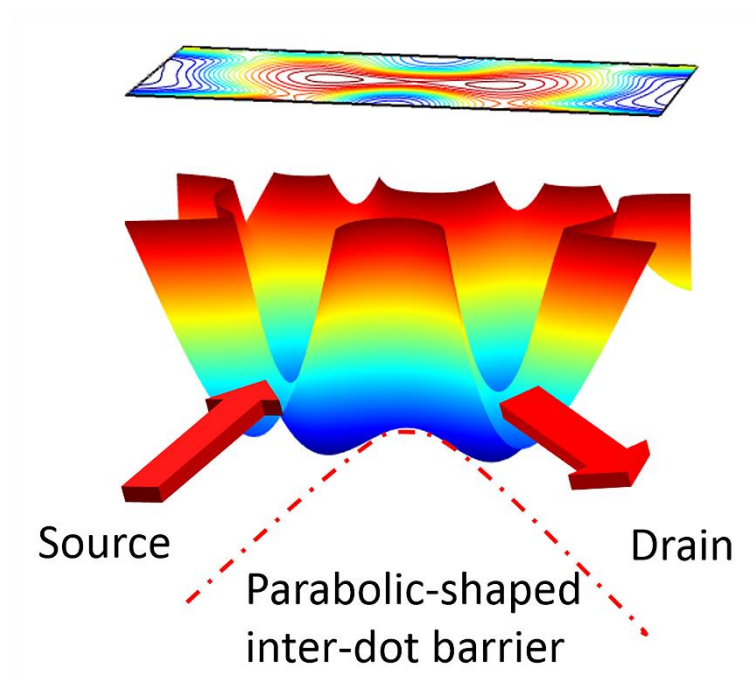


fig. S4. COMSOL simulation of the interdot barrier.

4. COMSOL simulation for different values of V_{DM}

When tuning V_{DM} to more negative values, the inter-dot potential barrier arises, leading to the reduction of the coupling strength between the dots (as shown in Fig. 3). A COMSOL simulation is used to calculate the change of potentials for different values of V_{DM} , while other gate voltages remain fixed, as shown in fig. S5. The inter-dot barrier increases when tuning V_{DM} more negative. Meanwhile, the dot confinement potential remains almost unaffected.

The schematic diagram of the evolution of such double-dot to single-dot transition of the confining potential at the crossline in fig. S5 is shown in Fig. 3, C to E. Such simulation results agree well with the experiment results.

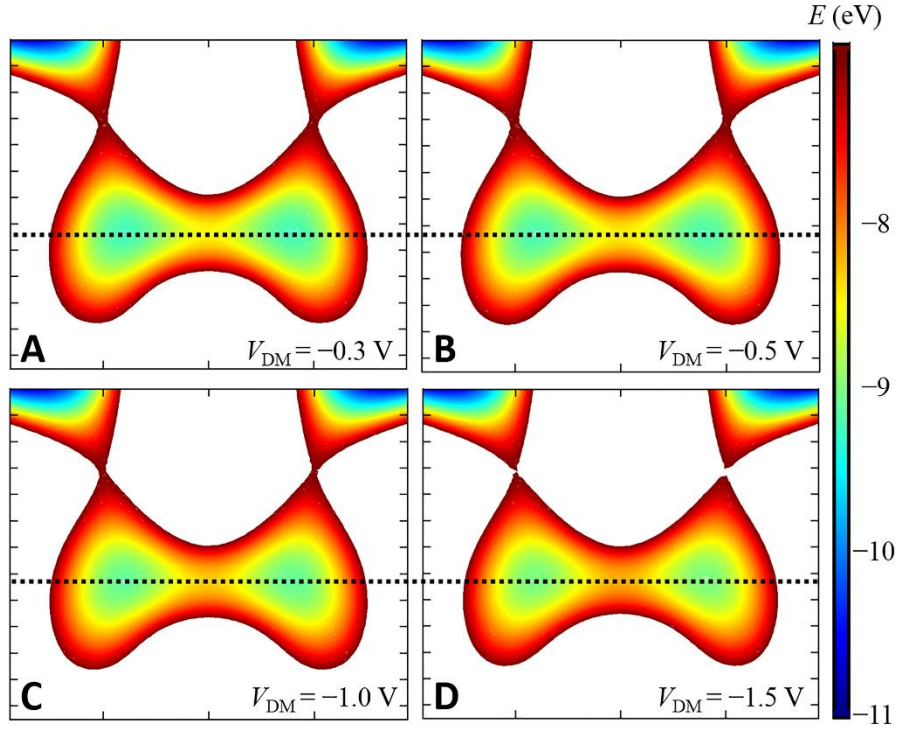


fig. S5. COMSOL simulation on the potential well distribution for different values of V_{DM} . COMSOL simulation on the potential-well distribution of the closed contours shown in Fig. 2D based on the designed pattern for $V_{BG} = 30$ V, $V_{LP} = V_{RP} = 0$ V, $V_{LB} = V_{RB} = -1.5$ V, $V_{UM} = -2.1$ V, and $V_{DM} = -0.3$ V, -0.5 V, -1 V and -1.5 V for **A** to **D**, respectively.

5. Gate controllability in the low-density regime

Because of the different values of V_{BG} , the formation of the double quantum dot was dominated by different mechanisms, as shown in Fig. 4, D and E. At a relatively low Fermi energy (E_{F1}), the intrinsic and fabrication-induced impurities dominate the confining potentials of the transport behavior, which cannot be well controlled by electrostatic gating. The controllability of the electrostatic gates here is demonstrated in fig. S6, A to C. When tuning the value of V_{DM} and V_{UM} together over a wide range, the tunneling rate between the source/drain and the dot changes effectively, while the coupling strength of two quantum dots does not show any obvious signature of evolution.

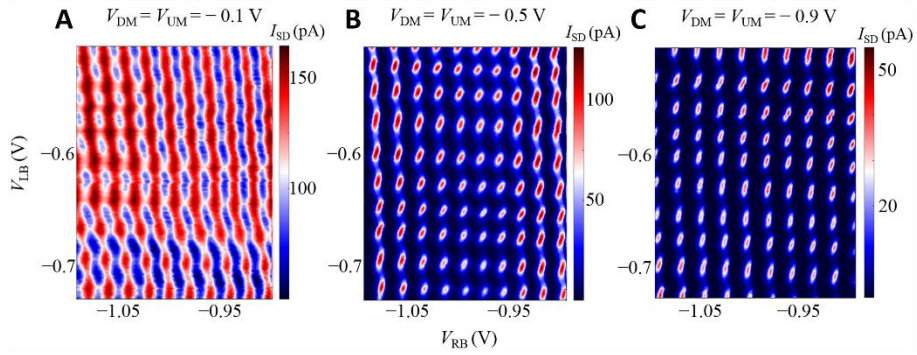


fig. S6. Gate controllability in the low-density regime. Current through the double quantum dot versus V_{LB} and V_{RB} applied to the gates LB and RB for $V_{BG} = 25$ V, $V_{LP} = V_{RP} = 0$ V, bias voltage at $V_{SD} = 100$ μ V and $V_{DM} = V_{UM} = -0.1$ V, -0.5 V, and -0.9 V for A to C, respectively.